

論文 / 著書情報  
Article / Book Information

Title	Centrifuge testing to investigate effects of partial saturation on the response of shallow foundation in liquefiable ground under strong sequential ground motions
Authors	Ritesh Kumar, Kazuki Horikoshi, Akihiro Takahashi
Citation	Soil Dynamics and Earthquake Engineering, Vol. 125, 105728
Pub. date	2019, 10
DOI	<a href="http://dx.doi.org/10.1016/j.soildyn.2019.105728">http://dx.doi.org/10.1016/j.soildyn.2019.105728</a>
Creative Commons	See next page.
Note	This file is author (final) version.

# License



**Creative Commons: CC BY-NC-ND**

**Title:**

Centrifuge testing to investigate effects of partial saturation on the response of shallow foundation in liquefiable ground under strong sequential ground motions

**Authors:**

Ritesh Kumar <sup>a</sup>, Kazuki Horikoshi <sup>b</sup>, and Akihiro Takahashi <sup>c\*</sup>

<sup>a</sup> Graduate Student

Department of Civil and Environmental Engineering

Tokyo Institute of Technology

Email: [kumar.r.aa@m.titech.ac.jp](mailto:kumar.r.aa@m.titech.ac.jp)

<sup>b</sup> Assistant Professor

Department of Civil and Environmental Engineering

Tokyo Institute of Technology

Email: [horikoshi.k.aa@m.titech.ac.jp](mailto:horikoshi.k.aa@m.titech.ac.jp)

<sup>c</sup> Professor (\*Corresponding author)

Department of Civil and Environmental Engineering,

Tokyo Institute of Technology

2-12-1-M1-3 Oh-okayama, Meguro, Tokyo 152-8552, Japan

Tel: +81-(0)3-5734-2593 Fax: +81-(0)3-5734-3577

Email: [takahashi.a.al@m.titech.ac.jp](mailto:takahashi.a.al@m.titech.ac.jp)

**Soil Dynamics and Earthquake Engineering, 125, 105728, 2019**

**Official URL:**

<https://doi.org/10.1016/j.soildyn.2019.105728>

## 27 **Abstract**

28 Induced partial saturation is one of the novel techniques to increase the liquefaction resistance of  
29 saturated sandy ground. Nonetheless, a limited number of experimental studies are available on the  
30 delineation of this method. Moreover, the performance of induced partial saturation under sequential  
31 ground motions is poorly understood. Dynamic centrifuge experiments are carried out to investigate  
32 the effects of partial saturation on the response of shallow foundation resting on liquefiable ground  
33 under sequential ground motions. Centrifuge models consist of two distinct shallow foundations and  
34 associated superstructures resting on a liquefiable uniform sand layer. The drainage-recharge method  
35 is used to induce partial saturation in the model ground. Compressibility change of pore fluid and  
36 alteration of ground permeability because of induced air voids, affect the deformation mechanism of  
37 the ground-foundation system. Assessment of maximum potential volumetric compressibility of pore  
38 fluid because of induced air voids is essential to understand the effectiveness of induced partial  
39 saturation. Centrifuge test results signify that the induced partial saturation reduces the overall  
40 deformation of the foundation-structure system. However, slightly amplified kinematic seismic  
41 demand is observed at superstructures in case of partially saturated ground in comparison with fully  
42 saturated ground.

43

## 44 **Keywords**

45 Centrifuge model test, excess pore water pressure, induced partial saturation, liquefaction, sequential  
46 ground motion, settlement, shallow foundation

47

## 48    **1. Introduction**

49    Liquefaction, a well-known phenomenon has been a topic of curiosity and complex experimentation  
50    among the geotechnical earthquake engineers and researchers all over the world since the past few  
51    decades. Liquefaction primarily occurs in the saturated loose cohesionless soil during dynamic/cyclic  
52    loading. During liquefaction, soil loses its shear strength due to excessive build-up of pore water  
53    pressure leading to ground failure, and sometimes even collapse of associated structures. Soil  
54    liquefaction and related ground failure have been extensively studied by many researchers [1-7].  
55    Liquefaction has caused damage to the built environment to a great extent. For instance, a significant  
56    part of the Christchurch city in New Zealand was devastated by soil liquefaction during the 2011  
57    Christchurch earthquake in terms of the structural settlement, tilting, and lateral spreading of the  
58    ground [6, 7]. In the 1964 Niigata and the 1990 Luzon (Philippines) earthquakes, most of the damaged  
59    buildings were two to four stories built on shallow foundations and relatively thick and uniform  
60    deposits of clean sand. Reports presented in many studies [8-10] described the role of liquefaction in  
61    the damage of buildings, specifically in the reclaimed land during the 2011 Tohoku earthquake.  
62    Numerous sand boils and large ground settlement, as well as the settlement/tilting of the wooden  
63    houses and reinforced concrete buildings supported on spread foundation, were seen throughout the  
64    affected area.

65    Soil remediation measures are requisite for liquefaction prone sites. In recent years, many researchers  
66    have explored liquefaction mitigation techniques that are different from commonly available practices  
67    as presented in reports by Mitchell et al., and Seed et al. [11-13]. Among those newly developed  
68    methods, induced partial saturation is one of the novel techniques to increase the liquefaction resistance  
69    of liquefiable ground. Partial saturation is achieved by artificially introducing the gas bubbles into soils.  
70    Several methods have been adopted to induce partial saturation within the ground such as water  
71    electrolysis [14], drainage-recharge [14, 15], chemical sodium perborate [16], biogas [17] and air  
72    injection [18, 19].

Laboratory experiments were performed by many researchers [20, 21] to understand the performance of induced partial saturation. The results showed that even a small change in the degree of saturation could increase the liquefaction resistance of liquefiable soil considerably. The inclusion of air voids within the saturated ground (to make it partially saturated) tend to decrease the overall bulk modulus and increase the compressibility of the pore fluid, which makes the development of excess pore water pressure less under cyclic shearing compared to the fully saturated condition. In this study, the drainage-recharge method is used to induce the partial saturation within the ground.

A comprehensive investigation is required to understand the effectiveness of induced partial saturation to mitigate the liquefaction effects on a shallow foundation. The effectiveness of air voids under multiple shaking, partial drainage effects on the evolution of excess pore water pressure, post-liquefaction behavior and soil-foundation-structure inertial and kinematic interaction are essential to assimilate to avail the maximum benefits of this technique. For that purpose, two dynamic centrifuge experiments are carried out to examine the performance of induced partial saturation to mitigate the liquefaction effects on shallow foundation under strong sequential ground motions.

## **2. Centrifuge Test Program**

Dynamic centrifuge tests are performed to investigate the effectiveness of induced partial saturation to mitigate the liquefaction effects on a shallow foundation. Dynamic centrifuge tests are carried out utilizing the Tokyo Tech Mark III centrifuge facility [22] having a radius of 2.45 m, at a centrifugal acceleration of 40 g ( $N=40$ ). Presented centrifuge tests simulate the prototype saturated soil deposit of 10 m depth. The model ground is prepared using the Toyoura sand (properties are shown in Table 1) with a relative density; of 50% by the air-pluviation method. The sand hopper is precisely calibrated in terms of the falling height and pouring rate to ensure the consistency of relative density for different model grounds. A flexible laminar container with inner dimensions of 600 x 250 x 438 mm (model scale) in length, width, and height respectively, is used to frame the models. The laminar box is

98 composed of many aluminum rectangular alloy rings which allow the movement along with soil mass  
99 which helps to create a flexible boundary and ensure the uniform dynamic shear stresses within the  
100 model ground during the dynamic excitation.

101

## 102 *2.1 Model foundation-structure system*

103 The scope of this paper is to evaluate the effectiveness of induced partial saturation for the isolated  
104 shallow foundation associated with temporary kind of structures resting on liquefiable ground.  
105 Therefore, two different types of superstructures (as shown in Fig. 1) are considered, in which left unit  
106 represents a typical Buffer Tank (BT), and right unit represents Flare Stack (FS). BT and FS (properties  
107 are shown in Table 2) impose an average bearing pressure of 51.2 kPa and 71.2 kPa respectively at 0.8  
108 m below the surface of the model ground in prototype scale as shown in Fig. 1. BT is a kind of storage  
109 tank, and FS is typically used to burn the unusable waste. They are generally mounted on an isolated  
110 shallow foundation. These two different structures are used to understand the rocking behavior  
111 (anticipated for FS as being the taller structure) of the structures during the shaking. Also, the  
112 effectiveness of induced air-voids is investigated under different bearing pressure with the help of BT  
113 and FS foundation-structure system. Moreover, the use of two different structures ensured the  
114 credibility of the evaluated performance of induced partial saturation. The height of prototype targeted  
115 structures, i.e. BT and FS are 15 m and 32 m respectively, having distributed mass along the height. In  
116 the model scale, the height of both BT and FS (after scaling down for  $N = 40$ ) turned out quite  
117 disproportionate concerning the laminar container size. Therefore masses are lumped at the middle of  
118 both BT and FS to ensure the fundamental design periods of BT and FS (0.4s and 0.5s, respectively).  
119 This improvisation reduced the height of BT and FS by 50.10% and 56.25 % respectively.

120

## 121 *2.2 Model ground preparation*

122 Flow charts of model ground preparation for both fully saturated and partially saturated model grounds

are shown in Fig. 2. Initially, the water tightness is ensured to avoid any fluid leakage from the laminar container during the experiment. Inner sides of the laminar box are covered with the polyethylene sheet to prevent any sand particles jamming between the alloy rings. Then sand is poured with the help of a sand hopper which is manually moved forth and back to achieve the uniform level ground at calibrated falling height and pouring rate. The transducers are carefully placed at desirable locations (see Fig.1 and Table 3) during the model ground preparation. The model is saturated with the viscous fluid, i.e., a mixture of water and 2 % Metolose (Hydroxypropylmethyl cellulose) by weight of water, to achieve a viscosity about 40 times that of water. This solution is used to ensure the compatibility of prototype permeability of the soil and to set up the affinity between dynamic and diffusion scaling laws [23]. The fully saturated model ground is prepared by dripping the de-aired Metolose solution slowly from the top of the container under a vacuum of 760 mmHg over the sponges at the surface of the model ground. The dripped solution slowly moves downward and saturates the model ground uniformly. The saturation is continued until the water table (Metolose solution table) reaches up to the top surface of the model ground. This saturation process for both the models took approximately 48 hours to complete. After the saturation, superstructures (BT and FS) are mounted over the footings and placed on the model ground at desirable locations (as shown in Fig. 1). It is to be noted that the wind speed at 40 g is tremendous which might cause turbulence to the FS because of comparatively large height. Therefore a wind casing is prepared to cover it as shown in Fig. 3.

### 2.3 Air induction

The drainage-recharge method is used to prepare the partially saturated model ground. Initially, the model ground is prepared and saturated as described in the Subsection mentioned above. After the saturation, the laminar box is taken out from the vacuum chamber. Then, the partial saturation is induced at 1g as follows (Fig. 2): In the first step, the Metolose solution is drained out from the model ground which turns the model into moist state and entrapped some amount of the air voids inside it. In



step 2, the drained-out Metolose solution is dripped back slowly on the sponges at the surface of the model ground in open air. The recharging is continued until the water table reaches back to the top surface of the model ground. It is to be noted that this time some amount of Metolose solution is left out because of entrapped air even though the water table reaches up to the top surface. The process mentioned in step 2 is repeated three times to ensure the uniformity of air voids entrapped within the model ground. Each time it took almost 4 hours to complete the drainage-recharge cycle. The overall degree of saturation within the partially saturated model ground is estimated by  $W_2/W_1$ , where  $W_2$  and  $W_1$  are the amounts of Metolose solution used in preparing the partially saturated and fully saturated model ground respectively. Due care is taken to estimate the degree of saturation for both fully saturated and partially saturated model grounds (tabulated in Table 4) using mass, volume and density relationships. However, it is worth noting that certain errors still happen to have a scope as mentioned by Kutter [24].

#### *2.4 Water table and effective stress*

The location of the water table is estimated using pore pressure readings of many pore pressure transducers at 40g to avoid/minimize any possible error. Estimated water tables for fully saturated and partially saturated model grounds are found to be at 0.7 m and 0.9 m respectively, below the surface of the ground in prototype scale. The vertical effective stress is one of the fundamental factors which determines the soil behavior. All measurable effects of change of stress, such as compression, distortion and a change of shearing resistance, are due exclusively to changes of effective stress [25]. The initial effective stress is calculated (as tabulated in Table 3) by subtracting the pore water pressure from the total stress. Vertical stress at desirable depths because of foundation-structure is calculated using Boussinesq's method which further is used to evaluate the vertical effective stress distribution within the ground.

## 2.5 Testing procedure

After finishing the saturation process, the model is mounted on the shaking table at centrifuge lab facility. Before applying the ground motions, the centrifuge model is tested against a white noise (WN1) as shown in Fig. 4 to understand the dynamic characteristics of the system. Fig. 5 shows the transfer function which is estimated as the ratio of acceleration obtained at the top of superstructures (A8 and A9 as shown in Fig. 1) to the white noise acceleration recorded at the base of the centrifuge model ground (A1) in the frequency domain. The fundamental periods obtained during the experiments are 0.42 and 0.37 s for BT, and 0.56 and 0.58 s for FS corresponding, respectively, for fully saturated and partially saturated model grounds in prototype scale. Natural periods of BT and FS obtained for both the models are very close to the design periods (as mentioned in Table 2). Ground motion recorded at Hachinohe Port during the 1968 Tokachi-Oki earthquake (NS component) is used as the first dynamic excitation after the white noise (WN 1). Enough time is given for full dissipation of excess pore water pressure before applying the second/sequential earthquake ground motion. Design earthquake motion for highway bridges in Japan (2-I-I-3, NS component) recorded at the ground surface near New Bansuikyo Bridge, Tochigi during the 2011 Tohoku Earthquake is used as the sequential ground motion to examine the foundation behavior under large earthquake. Model grounds configuration and the description of applied shakings are tabulated in Table 4. Fig. 6 shows the acceleration time histories, Fourier spectra and Arias intensity [26] of the input base motions for fully saturated and partially saturated model grounds. Exact simulation of ground motion in the centrifuge is quite complicated. Many trials were made to finalize the simulated shakings (of both Tokachi-Oki and Tohoku ground motions) before performing the centrifuge experiment. It is imperative that the simulated ground motions agree well in time and frequency domain as well as depict alike Arias intensity to ensure the fair comparison between test results of fully and partially saturated model grounds. Base motions shown here are presented after having baseline correction and filtering. Filtering is performed in the frequency domain using the bandpass Butterworth filter with corner

198 frequencies of 0.3Hz and 10 Hz respectively in prototype scale. It is evident that the simulated  
199 waveforms for both cases possesses similar intensity and are in good agreement both in time as well  
200 as frequency domain.  
201

### 202 **3. Test Results and Discussion**

#### 203 *3.1 Evolution of excess pore water pressure*

204 All the test results shown in the following sections are in the prototype scale unless mentioned  
205 otherwise. Excess pore water pressure (EPWP) time histories are obtained at several desirable locations  
206 as shown in Fig. 1. Evolution of EPWP (generation and dissipation trend), plays a vital role in the  
207 understanding of the liquefaction phenomena. Soils at certain depth undergo liquefaction if the excess  
208 pore water pressure ratio ( $r_u$ ) which is calculated by dividing the generated EPWP by the initial vertical  
209 effective stress at the respective depth, approaches to unity. Table 3 shows the initial vertical effective  
210 stress at all transducers locations for both fully saturated and partially saturated model grounds.

211 Fig. 7 depicts the EPWP time histories for the fully saturated and partially saturated model grounds  
212 when subjected to Tokachi-Oki ground motion. At P1 (Level 1), the EPWP time histories are almost  
213 same in both the cases in terms of maximum magnitude; though, the dissipation trend is marginally  
214 delayed in case of partially saturated model ground. As the hydrostatic pressure at Level 1 (base of the  
215 model ground) is significantly high, there might be a possibility of volume change/dissolution of air  
216 voids. Therefore, both fully saturated and partially saturated model grounds exhibit similar behavior  
217 in terms of generated EPWP trends at the base of the model ground which is further elaborated in the  
218 following Subsection. At P2 and P4 (Level 3), the presence of air voids within the partially saturated  
219 model ground significantly delayed the generation and dissipation of EPWP in comparison with the  
220 fully saturated model ground. This behavior occurs primarily because of the increase in compressibility  
221 of the air and pore fluid mixture in case of partially saturated model ground [14]. In addition, induced  
222 partial saturation reduced the overall permeability of partially saturated ground. This also justifies the

223 behavior of the slower rate of generation and dissipation of EPWP as shown in [Fig. 7](#). At this level  
224 (Level 3), the maximum magnitude of generated EPWP has surpassed the liquefaction state line (i.e.  
225  $r_u=1$ ) in case of fully saturated model ground whereas the liquefaction state is not observed in case of  
226 the partially saturated model ground. Similar behavior of EPWP generation and dissipation is observed  
227 at P6 (Level 4). In case of fully saturated model ground, liquefaction state is achieved at P6 whereas,  
228 the maximum magnitude of EPWP in case of the partially saturated model ground is far below the  
229 liquefaction state line. Unfortunately, the pore water pressure transducers P3 and P5 did not work  
230 correctly because of some unforeseen reasons and hence are not shown in [Fig. 7](#).

231 At shallower depth (Level 5), EPWP time histories at P7 share almost the same magnitude of maximum  
232 EPWP for both fully saturated and partially saturated model grounds. However, the generation and  
233 dissipation rate of EPWP at P7 is delayed in case of partially saturated model ground in comparison  
234 with the fully saturated model ground. The possible explanation for this unusual behavior at P7 might  
235 be non-uniformity of partial saturation in the vicinity of Flare Stack (FS) footing. At P9 (Level 5), the  
236 maximum magnitude of generated EPWP is significantly less in case of partially saturated model  
237 ground in comparison with the fully saturated model ground. The liquefaction state is not achieved at  
238 P7 (under FS) and P9 (under BT) because of large vertical effective stress due to the foundation-  
239 structure system. It is interesting to note that the maximum magnitude of EPWP at P8 (Level 5) in case  
240 of the fully saturated model ground is more than the one at P7 and P9, even though the vertical stress  
241 at P8 is less than P7 and P9. The reason for this is the flow of pore fluid and settlement caused under  
242 the shallow foundation [\[13, 27\]](#). Both BT and FS foundation has influence zone of large confining  
243 stress in the vicinity of foundation, and because of vertical hydraulic gradient setup during dynamic  
244 excitation, the pore fluid is bound to flow nearby the model centerline. The availability of significant  
245 amount of migrated pore fluid for a long time resulted in more EPWP at P8 than P7 and P9.

246 [Fig. 8](#) depicts the EPWP time histories for both fully saturated and partially saturated model grounds  
247 when subjected to Tohoku ground motion. It is evident from [Fig. 8](#) that whole model ground gets

liquefied except in the vicinity of FS foundation (at P7) in case of fully saturated model ground. However, induced partial saturation can avoid the liquefaction state at P6 (Level 4) and P7 and P9 (Level 5) in case of the partially saturated model ground. During Tohoku ground motion, the overall performance of partially saturated ground is diminished in comparison with the one witnessed during Tokachi-Oki ground motion. Tohoku earthquake is stronger than the Tokachi-Oki in terms of both peak acceleration and duration. Also, there is a considerable possibility that a few percentages of air voids might have disintegrated/dissolved during Tokachi-Oki earthquake because of pore fluid migration in the liquefied zone (further elaborated in Subsection 3.2) and due to the deformation of the model ground.

Pore pressure transducers (PPTs) at a shallower depth (P7-P9) exhibit maximum EPWP quite after the shaking period in case of partially saturated model ground during both Tokachi-Oki and Tohoku ground motion as shown in Figs 7-8. The reason for this is the slower rate of water flow from the deeper portion of the model ground in case of partially saturated ground. It is to be noted that all PPTs show a small magnitude of the residual EPWP in dissipation phase at 5000 s except at P1 (Figs. 7-8). This is associated with the fact that the PPTs experienced a marginal settlement during the shakings which changed the overall void ratio (probably decreased) and the marginal rise of the water table. This inevitable settlement of PPTs during Tokachi-Oki ground motion changed the initial vertical effective stress condition at the location of PPTs for Tohoku ground motions. However, the initial vertical effective stress is assumed to be constant for both the ground motions (Tokachi-Oki and Tohoku earthquake) at different levels in the model ground as mentioned in Table 3 for the sake of brevity.

268

### 3.2 Air void dissolution/collapse during shaking

Air voids are introduced using the drainage-recharge method to induce partial saturation within the model ground in this study. The detailed process of air induction is already described in Subsection 2.3. It is to be noted that the model grounds are prepared in 1g condition and the calculated degree of

273 saturation is certain to change at 40g environment within the partially saturated model ground.  
 274 Introducing Boyle's law and assuming air voids to be isolated and soil grains to be incompressible, the  
 275 distribution of the degree of saturation is estimated within the partially saturated model ground at 40g.  
 276 Fig. 9 depicts that the degree of saturation increases (significantly) at the deeper portion of the model  
 277 ground due to high hydrostatic pressure condition. This is also confirmed by the evolution of excess  
 278 pore water pressure (EPWP) as explained in the previous Subsection. There are two governing factors  
 279 by which the induced partial saturation can increase the liquefaction resistance of the ground. The first  
 280 factor is the increase in the compressibility of the pore fluid due to the air voids entrapped within the  
 281 pore fluid. This mechanism helps to restrict the rate of development of excess pore water pressure  
 282 during cyclic loading which is also witnessed during the EPWP build-up stage in the experiment as  
 283 depicted from Figs.7-8. The second one is matric suction which is not significant in the case of  
 284 liquefiable soil as explained by Bishop and Blight [28]. By implementing the above stated Boyle's law,  
 285 the maximum potential volumetric compressibility (strain) within the model ground can be estimated  
 286 using the evolution of EPWP during the shaking [21, 29]. Consider a fully saturated soil mass  
 287 comprising incompressible soil particles and pore fluid. For a small change in pressure, the volumetric  
 288 strain in soil mass will be zero under undrained condition. However, the soil mass with air voids  
 289 (partially saturated case) will undergo considerable volumetric strain (potential volume  
 290 compressibility) under the same conditions. This potential volume compressibility of soil mass is  
 291 solely due to the inclusion of air voids as the water and sand particles are assumed to be incompressible.  
 292 The empirical equation proposed by Okamura and Soga [21] is used to estimate the potential  
 293 volumetric compressibility which required the parameters such as the degree of saturation (Fig. 9),  
 294 initial vertical effective stress (Table 3), maximum excess pore water pressure, and the initial void ratio  
 295 (Table 1).  
 296 Fig. 10 shows the maximum potential volume compressibility because of air voids induced within the  
 297 partially saturated model ground during white noise 1 (WN1, before Tokachi-Oki ground motion) and

white noise 2 (WN2, after Tohoku ground motion). The maximum potential volumetric strain depends on several factors such as void ratio, the evolution of EPWP, dynamic shaking, vertical effective stress and degree of saturation. Considering these factors and to evaluate the available potential volumetric compressibility before and after the main shakings, four locations (at P2, P4, P5, and P6 as shown in Fig.1) are considered during the white noises. The reason for selecting pore pressure locations at Levels 3 and 4 (at P2, P4, P5, and P6) is to avoid/minimize the influence of an abrupt change in void ratio and degree of saturation during and after the shaking. Both white noise shakings (WN1 and WN2) are alike as shown in Fig. 10 and possess almost same intensity. It is evident from Fig. 10 that the availability of maximum potential volumetric compressibility because of induced air voids during WN1 is relatively more than that available during WN2. This is associated with the fact of air void dissolution/collapse during Tokachi-Oki and Tohoku ground motion which is also witnessed from the EPWP time histories (Fig. 8) as explained in the previous Subsection. However, the available capacity of potential volume compressibility is quite significant even after the strong Tohoku ground motion (corresponds to WN2) which signifies the novelty of induced partial saturation to increase the liquefaction resistance of the partially saturated ground.

### 3.3 Permeability of partially saturated ground

Fig. 11 shows the soil-water characteristic curve for Toyoura sand [30]. The permeability of partially saturated model ground at a different degree of saturation (along the depth as shown in Fig. 9) is estimated using van Genuchten model [31]. Initially, the van Genuchten model parameters for Toyoura sand are calculated using the experiment data retrieved from Unno et al. [30]. Then, the variation of the degree of saturation along the depth of the partially saturated model ground (Fig. 9) is used to estimate the volumetric water content. After that, the effective degree of saturation  $S_e$  [31] is determined and used to calculate the permeability coefficient. The permeability coefficient plotted in Fig. 12 is the ratio of  $K_{P\_sat}$  (permeability of partially saturated ground) and  $K_{F\_sat}$  (permeability of fully

saturated ground). For detail procedure of permeability estimation, readers are suggested to refer Unno et al. [30] and Fredlund et al. [32]. It is evident from Fig. 12 that the permeability within the partially saturated model ground reduced significantly as much as up to 40 % to 60 % of the permeability of fully saturated model ground. 1-D consolidation analysis is also performed to estimate the overall relative permeability of the partially saturated ground. With appropriate boundary conditions and an initial value of pore water pressure at the end of the shaking (or at the beginning of dissipation phase), the dissipation curve of pore water pressure is estimated at P2 and P4 for both fully saturated and partially saturated grounds during Tokachi-Oki ground motion. The dissipation phase of pore water pressure is governed by the coefficient of consolidation which includes soil permeability, compressibility, and unit weight of pore fluid. The estimated dissipation curves of pore water pressure at P2 and P4 are fitted with the centrifuge test results by changing the permeability values [33]. Then the average permeability coefficient ( $K_{P\_sat}/K_{F\_sat}$ ) for P2 and P4 is obtained which is found to be 0.73 during the Tokachi-Oki ground motion. This also corroborates the fact that induced air-voids reduce the overall permeability of the partially saturated ground.

### 3.4 Settlement behavior

Fig. 13 depicts the settlement observed at BT and FS footings during Tokachi-Oki ground motion. Two laser displacement transducers (LDTs) are used to record the footing settlement for BT (LDTs 1, and 2) and FS (LDTs 3, and 4). It is evident that both BT and FS footings undergo excessive settlement in case of fully saturated ground. The foundations begin to settle immediately after the shaking began and continued even after the shaking ceased. BT footing exhibits large magnitude of differential settlement (the difference between the settlements of both sides of the footing) by the side of LDT1 in case of the fully saturated ground; whereas, FS footing exhibits comparatively smaller but significant magnitude of differential settlement in case of partially saturated ground. Seismic demand, relative density, liquefaction state, foundation height/width ratio, bearing pressure and overall drainage in the



vicinity of the foundation are few of the factors to mention which govern the overall liquefaction induced settlement mechanism of shallow foundation [27]. In addition, the non-uniform degree of partial saturation in the ground might be responsible for the differential settlement of foundation-structure system in case of partially saturated ground. A sudden jump in LDT2 reading (see \* in Fig. 13) in the very beginning of shaking is apparent which might be because of movement of the sensor holder/plate as such sudden change could not be seen in all other sensors.

Fig. 14 depicts the settlement observed at BT and FS footing during Tohoku ground motion. In case of fully saturated ground, both BT and FS experienced collapse kind of behavior (from the visual inspection after the experiment, it is found that both BT and FS had struck to the surrounding guide plate). As explained earlier, during Tokachi-Oki ground motion, BT footing exhibits the significant amount of differential settlement in the direction of LDT1 in case of fully saturated ground. The rotational tilting (as it seems to have happened from Fig. 14) occurred after the Tohoku ground motion, and BT footing concludes with excessive differential settlement by the side of LDT2. This unusual behavior of BT during Tohoku ground motion in case of fully saturated model ground might have happened because of the soil flow (traces were observed after the experiment) over the location of LDTs 1, 2 and 4 during Tohoku ground motion because of liquefaction. In that case, the LDTs (1, 2 and 4) readings, especially after the soil overflow (dashed lines in Fig. 14), are not reliable in case of fully saturated model ground for Tohoku ground motion. It is evident from Figs. 13-14, that the overall performance of the partially saturated ground for both the footings and associated superstructures is better than the fully saturated ground.

Fig. 15 shows the cumulative average settlement of BT and FS footings during and after the shakings (Tokachi-Oki and Tohoku ground motions). It is evident that footings undergo significant co-shaking settlement (settlement occurred during shaking) in case of fully saturated model ground during both Tokachi-Oki and Tohoku ground motion. Shear-induced deformation is the governing factor for co-shaking settlement, and it can be seen from Fig. 15 as the overall vertical settlement of FS is

significantly large compared to the vertical settlement of BT. The shear strength of soil in the vicinity of the foundation start to mobilize because of generation of excess pore water pressure (reduction in mean vertical effective stress) and hence shear-induced co-shaking settlement is apparent. The induced partial saturation can mitigate the shear-induced deformation as the co-shaking settlement in case of the partially saturated ground is less in comparison with the fully saturated ground. Volumetric strains due to partial drainage and development of post-liquefaction/shaking reconsolidation strains are the prime responsible factors associated with the post-shaking settlement. It is evident from Fig. 15 that the post-shaking settlement is significantly mitigated by the presence of air voids in case of partially saturated model ground. Unfortunately, the post-shaking readings of LDTs in case of fully saturated ground are not reliable during Tohoku ground motion as discussed earlier and hence are not shown in Fig. 15. Fig. 16 depicts the surface settlement (topography) measured after the centrifuge experiments. The surface settlement is shown in Fig. 16 is the cumulative response during all the shakings. Larger the bearing pressure more is the settlement in the vicinity of the foundation for both fully saturated and partially saturated ground. It is evident that the overall surface settlement is significantly less in case of partially saturated ground in comparison with fully saturated ground.

### *3.5 Kinematic and inertial interaction between the model ground-foundation-structure system*

It is a well-established fact that during the dynamic excitation soils undergo deformations which are further foisted on the foundation. During the seismic loading, the wave propagates through the soil media which altered in the vicinity of the structure. This well-known phenomenon of soil-structure interaction dominantly governs the structure behavior in the liquefiable ground. Inertial interaction is not significant in case of liquefiable ground because the soil is assumed to behave as a seismic isolator to the foundation [34]. However, superstructure's dynamic properties that control inertial interaction (e.g., mass, stiffness, height to width ratio) have shown significant influence on the evolution of the pore water pressure, settlement trend, tilt potential, which in turn, affect the overall

398 performance of superstructure [35].

399 Fig. 17 depicts the acceleration time histories recorded at several locations on/within foundation-  
400 superstructure and model ground (see Fig. 1). The position of A5 (at Level 5) along the model  
401 centerline is considered as the far-field (FF). Although A5 is placed significantly away from, and  
402 approximately at the same level of the base of the footings of both structures, some interaction is still  
403 expected to happen due to spacing constraints between the structures. Acceleration records measured  
404 at A5 showed the significant amount of de-amplification in acceleration time histories for both fully  
405 saturated and partially saturated model grounds during Tokachi-Okai and Tohoku ground motions.  
406 Significant de-amplified acceleration time history of A5 also consolidate the fact that the model ground  
407 exhibits considerable softened state during Tokachi-Okai and Tohoku ground motions. Partially  
408 saturated ground shows relatively less de-amplification in comparison with the fully saturated ground  
409 at all locations except at A7 and A9 in case of Tohoku ground motion. This explains that the partially  
410 saturated model ground exhibits more liquefaction resistance (relatively less model ground softening)  
411 in comparison with the fully saturated model ground. Similar observations of acceleration records were  
412 made by Zeybek and Madabhushi [36]. During Tohoku ground motion, acceleration time histories  
413 recorded at the foundation and superstructure of FS (A7 and A9) showed the spikes in case of fully  
414 saturated ground. The reason for this might be the excessive settlement of the foundation [27]. Also,  
415 larger acceleration spikes at the FS might be observed because of soil dilation and re-stiffening caused  
416 by excessive soil flow under the shallow foundation.

417 To examine the influence of the kinematic and inertial interaction on foundation, Fourier amplitude  
418 spectra (FAS) of acceleration records at footings and far-field is obtained as shown in Fig. 18. The FAS  
419 representation of acceleration records can give an insight of amplification/attenuation between fully  
420 saturated and partially saturated ground at respective locations. The frequency content can be divided  
421 into two ranges; i.e., acceleration dominating ( $Fa$ ) and velocity dominating ( $Fv$ ) range as suggested by  
422 Borchardt [37]. It is evident that the FAS amplitudes for FF and BT are significantly large in case of

partially saturated model ground in comparison with the fully saturated ground during both Tokachi-Oki and Tohoku ground motions. The observed amplification is more dominating in the  $F_v$  frequency (0.5–2.0 Hz) range. This demonstrates that the partially saturated ground yield amplified seismic demand to the model ground-foundation system. However, the FAS trend for FS footing seems to be alike for both fully saturated and partially saturated grounds during Tokachi-Oki ground motion. Although, a marginal attenuation in FAS is observed for high frequency in case of partially saturated ground. The reason for this is alike model ground condition in the vicinity of FS footing as the degree of saturation is almost same for both fully saturated and partially saturated ground.

### *3.6 Strength/Stiffness mobilization of model ground*

[Fig. 19](#) depicts transfer functions (TFs) during white noise 1, Tokachi-Oki, and Tohoku ground motions. The ratio of acceleration records at A5 to A1 in the frequency domain is used to obtain the TFs. It is evident that the fundamental site frequency obtained for both fully saturated and partially saturated grounds during white noise 1 falls within the range of small-strain site fundamental frequency obtained by empirical equations [\[38\]](#), even though the soil response is highly nonlinear. This also implies that the fundamental site frequency of the model ground could be captured by appropriate white noise (usually a random small amplitude vibration having equal intensities at different frequencies, giving it a constant power spectral density). Shear wave velocity profile (within the ground using small strain shear pulse) is used in empirical equations to estimate the fundamental site frequency. The upper and lower bound of the fundamental frequency of the model ground (2.5~2.8 Hz) is determined by the estimated range of shear wave velocity (approximately 169 to 186 m/s) using empirical equations as mentioned above. Site fundamental frequencies obtained during Tokachi-Oki ground motion falls to 0.54 and 0.8 Hz for the fully saturated and partially saturated model ground respectively. The significant drop in site fundamental frequency occurred because of the softening of the model ground during Tokachi-Oki ground motion [\[39\]](#). It is evident that the extent of model ground softening is

relatively small in case of partially saturated ground in comparison with the fully saturated ground. However, both the model grounds exhibit nearly same trend of TFs during Tohoku ground motion. Back analysis of acceleration records, is performed to get the insight into the progression of shear strain within the model ground. Many studies justify the credibility of this method. Zeghal et al. [40]; Adalier and Elgamal [41] used the recorded lateral accelerations to evaluate shear stress and strain histories at different elevations within the ground. Brennan et al. [42] assessed the shear modulus and shear degradation curves for dry and saturated sand, soft clay from the acceleration histories obtained from the centrifuge tests. Fig. 20 depicts the shear strain developed along the centerline of the model ground between different levels (as mentioned in Table 3) during the centrifuge test for fully saturated and partially saturated grounds. At a shallower depth (between Levels 4 and 5), the shear strain developed within the partially saturated ground is significantly less in comparison with fully saturated ground. Similar behavior is observed between Levels 3 and 4. This behavior corroborates the fact that inclusion of air voids within the ground increases the liquefaction resistance of the ground. However, shear strain time histories between Levels 2-3 and Levels 1-2 are alike for both fully saturated and partially saturated grounds. The presence of air voids seems to have negligible effects at the deeper portion. Excess pore water pressure time histories obtained at the deeper portion (Figs. 7 and 8) also delineate the limitation of the presence of the air voids under higher stress level.

#### 4. Conclusions

Dynamic centrifuge experiments are carried out to investigate the effects of partial saturation on shallow foundation resting on liquefiable ground under sequential ground motions. The drainage-recharge method is used to induce partial saturation within the liquefiable ground. The response of partially saturated ground is compared with the fully saturated ground in terms of the evolution of excess pore water pressure at several locations, settlement time histories of footings, and kinematic and inertial interaction between soil-foundation-structure system. The observed slower rate of

generation and dissipation of excess pore water pressure in case of partially saturated ground, consolidate the fact that the compressibility of pore fluid increases because of inclusion of the air voids within the ground. Also, the partially saturated ground shows overall less permeability in comparison with the fully saturated ground. Partially saturated ground exhibited a significant amount of maximum potential volumetric compressibility of pore fluid after the strong Tohoku ground motion (sequential motion applied after Tokachi-Oki ground motion) which justify the efficacy of induced partial saturation. In case of fully saturated ground, the foundation-structure systems undergo excessive settlement with complete bearing failure under the foundation during Tohoku ground motion. Whereas, induced partial saturation can minimize the settlement of foundation-structure systems in case of partially saturated ground. The kinematic seismic demand experienced by foundation-structure systems is relatively large in case of partially saturated ground in comparison with fully saturated ground. Despite that fact, centrifuge experiments show promising results in favor of induced partial saturation to mitigate the liquefaction-induced effects on shallow foundation.

## **Acknowledgments**

The work presented in this paper is part of the collaborative research with the Nippon Steel & Sumikin Engineering. The authors would like to thank Dr Ece Eseller-Bayat, Istanbul Technical University, for useful discussions. Her visit to Tokyo Institute of Technology and the last author's visit to Istanbul Technical University were supported by Japan-Turkey Cooperative Education Program on Resilience Engineering for Energy and Urban Systems (funded by JSPS). The first author sincerely acknowledges the support provided by Monbukagakusho (Ministry of Education, Culture, Sports, Science, and Technology) scholarship for graduate students. The authors are also indebted to Mr. Sakae Seki, lab technician, Department of Civil and Environmental Engineering, Tokyo Institute of Technology for his tremendous contribution in the successful completion of centrifuge experiments.

## Reference

- [1]. Seed RB, Dickenson SE, Riemer MF, Bray JD, Sitar N, Mitchell JK, Idriss IM, Kayen RE, Kropp A, Hander Jr. LF, Power MS. Preliminary report on the principal geotechnical aspects of the October 17, 1989, Loma Prieta Earthquake. Rep. No. UCB/EERC-90/05, Earthquake Engineering Research Center, Uni. of California, Berkeley, 1990.
- [2]. Ishihara K, Haeri SM, Moinfar AA, Towhata I, Tsujino S. Geotechnical aspects of the June 20, 1990 Manjil Earthquake in Iran. *Soils and Foundations* 1992; 32(3):61–78. [https://doi.org/10.3208/sandf1972.32.3\\_61](https://doi.org/10.3208/sandf1972.32.3_61).
- [3]. Bardet JP, Oka F, Sugito M, Yashima A. The Great Hanshin Earthquake disaster. Preliminary Investigation Rep., Dept. of Civil Engineering Univ. of Southern California, Los Angeles, 1995.
- [4]. Sugito M, Oka F, Yashima A, Furumoto Y, Yamada K. Time-dependent ground motion amplification characteristics at reclaimed land after the 1995 Hyogoken Nambu Earthquake. *Engineering Geology* 2000; 56(1):137–150. [https://doi.org/10.1016/S0013-7952\(99\)00139-8](https://doi.org/10.1016/S0013-7952(99)00139-8).
- [5]. Krinitzsky EL, Hynes ME. The Bhuj, India, earthquake: lessons learned for earthquake safety of dams on alluvium. *Engineering Geology* 2002; 66(3):163–196. [https://doi.org/10.1016/S0013-7952\(02\)00049-2](https://doi.org/10.1016/S0013-7952(02)00049-2).
- [6]. Green RA, Cubrinovski M, Wotherspoon L, Allen J, Bradley B, Bradshaw A. Geotechnical reconnaissance of the 2011 Christchurch, New Zealand earthquake. *Geotechnical Extreme Events Reconnaissance (GEER) Report* 2011; 1(8).
- [7]. Cubrinovski M, McCahon I. Short term recovery project 7, CBD foundation damage. *Natural Hazards Research Platform*. Christchurch, New Zealand, University of Canterbury, 2012.
- [8]. Nakai S, Sekiguchi T. Damage due to liquefaction during the 2011 Tohoku earthquake. In *Proc. of the International Symposium for CSMID 2011*; 1-8.
- [9]. Bhattacharya S, Hyodo M, Goda K, Tazoh T, Taylor CA. Liquefaction of soil in the Tokyo Bay area from the 2011 Tohoku (Japan) earthquake. *Soil Dynamics and Earthquake Engineering*

2011; 31(11):1618-1628. <https://doi.org/10.1016/j.soildyn.2011.06.006>.

[10]. Tokimatsu K, Tamura S, Suzuki H, Katsumata K. Building damage associated with geotechnical problems in the 2011 Tohoku Pacific Earthquake. *Soils and Foundations* 2012;52(5): 956-974. <https://doi.org/10.1016/j.sandf.2012.11.014>.

[11]. Mitchell JK, Baxter CD, Munson TC. Performance of improved ground during earthquakes. In *Soil improvement for earthquake hazard mitigation* 1995;1-36.

[12]. Seed RB, Cetin KO, Moss RES, Kammerer AM, Wu J, Pestana JM, Reimer MF. Recent advances in soil liquefaction engineering and seismic site response evaluation 2001.

[13]. Zeybek A, Madabhushi SPG. Influence of air injection on the liquefaction-induced deformation mechanisms beneath shallow foundations. *Soil Dynamics and Earthquake Engineering* 2017; 97:266-276. <https://doi.org/10.1016/j.soildyn.2017.03.018>.

[14]. Yegian MK, Eseller-Bayat E, Alshawabkeh A, Ali S. Induced partial saturation (IPS) for liquefaction mitigation: experimental investigation. *J Geotech Geoenviron Eng, ASCE* 2007; 133(4):372–80. [https://doi.org/10.1061/\(ASCE\)1090-0241\(2007\)133:4\(372\)](https://doi.org/10.1061/(ASCE)1090-0241(2007)133:4(372)).

[15]. Takemura J, Igarashi R, Izawa J, Okamura M. Centrifuge Model tests on soil desaturation as a liquefaction countermeasure. In: *Proceedings of the 5<sup>th</sup> International conference on urban earthquake engineering*, Tokyo institute of technology. Tokyo, Japan; 2008; 269–274.

[16]. Eseller-Bayat E, Yegian MK, Alshawabkeh A, Gokyer S. Liquefaction response of partially saturated sands. I: experimental results. *J Geotech Geoenviron Eng, ASCE* 2013; 139(6):863–871. [https://doi.org/10.1061/\(ASCE\)GT.1943-5606.0000815](https://doi.org/10.1061/(ASCE)GT.1943-5606.0000815).

[17]. He J, Chue J, Ivanov V. Mitigation of liquefaction of saturated sand using biogas. *Géotechnique* 2013; 63(4):267–275. <http://dx.doi.org/10.1680/geot.SIP13.P.004>.

[18]. Tokimatsu K, Yoshimi Y, Ariizumi K. Evaluation of liquefaction resistance of sand improved by deep vibratory compactions. *Soils Found* 1990;30(3):153–158. [https://doi.org/10.3208/sandf1972.30.3\\_153](https://doi.org/10.3208/sandf1972.30.3_153).



- [19]. Okamura M, Ishihara M, Oshita T. Liquefaction resistance of sand deposit improved with sand compaction piles. *Soils Found* 2003; 43(5):175–187. [https://doi.org/10.3208/sandf.43.5\\_175](https://doi.org/10.3208/sandf.43.5_175).
- [20]. Yoshimi Y, Yanaka K, Tokimatsu K. Liquefaction resistance of a partially saturated sand. *Soils Found* 1989; 29(2):157–162. [https://doi.org/10.3208/sandf1972.29.3\\_157](https://doi.org/10.3208/sandf1972.29.3_157).
- [21]. Okamura M, Soga Y. Effects of pore fluid compressibility on liquefaction resistance of partially saturated sand. *Soils Found* 2006; 46(5):695–700. <https://doi.org/10.3208/sandf.46.695>.
- [22]. Takemura J, Kondoh M, Esaki T, Kouda M, Kusakabe O. Centrifuge model tests on double propped wall excavation in soft clay. *Soils and Foundations* 1999; 39(3):75-87. [https://doi.org/10.3208/sandf.39.3\\_75](https://doi.org/10.3208/sandf.39.3_75).
- [23]. Schofield AN. Dynamic and earthquake geotechnical centrifuge modelling. In: *Proceedings of International conference on recent advances in geotechnical earthquake engineering and soil dynamics*, University of Missouri-Rolla. MO, USA 1981;1081–1100.
- [24]. Kutter BL. Effects of capillary number, Bond number, and gas solubility on water saturation of sand specimens. *Can Geotech J* 2013; 50(2):133–144. <https://doi.org/10.1139/cgj-2011-0250>.
- [25]. Atkinson, J. *The mechanics of soils and foundations*. CRC Press 2007.
- [26]. Kayen RE, Mitchell JK. Assessment of liquefaction potential during earthquakes by Arias intensity. *Journal of Geotechnical and Geoenvironmental Engineering* 1997; 123(12):1162-1174. [https://doi.org/10.1061/\(ASCE\)1090-0241\(1997\)123:12\(1162\)](https://doi.org/10.1061/(ASCE)1090-0241(1997)123:12(1162)).
- [27]. Dashti S, Bray JD, Pestana JM, Riemer MR, Wilson D. Centrifuge testing to evaluate and mitigate liquefaction induced building settlement mechanisms. *J. Geotech. Geoenviron. Eng.* 2010 (a); 136(7):918–929. [https://doi.org/10.1061/\(ASCE\)GT.1943-5606.0000306](https://doi.org/10.1061/(ASCE)GT.1943-5606.0000306).
- [28]. Bishop AW, Blight GE. Some aspects of effective stress in saturated and partly saturated soils. *Geotechnique* 1963; 13(3):177-197. <https://doi.org/10.1680/geot.1963.13.3.177>.
- [29]. Marasini NP, Okamura M. Numerical simulation of centrifuge tests to evaluate the performance of desaturation by air injection on liquefiable foundation soil of light structures. *Soils and*

- 573 Foundations 2015; 55(6):1388-1399. <https://doi.org/10.1016/j.sandf.2015.10.005>.
- 574 [30]. Unno T, Kazama M, Uzuoka R, Sento N. Liquefaction of unsaturated sand considering the pore  
575 air pressure and volume compressibility of the soil particle skeleton. Soils and Foundations 2008;  
576 48(1):87-99. <https://doi.org/10.3208/sandf.48.87>.
- 577 [31]. Van Genuchten MT. A closed-form equation for predicting the hydraulic conductivity of  
578 unsaturated soils 1. Soil science society of America journal 1980; 44(5):892-898.
- 579 [32]. Wang B, Zen K, Chen GQ, Zhang YB, Kasama K. Excess pore pressure dissipation and  
580 solidification after liquefaction of saturated sand deposits. Soil Dynamics and Earthquake  
581 Engineering 2013, 49:157-164. <https://doi.org/10.1016/j.soildyn.2013.02.018>.
- 582 [33]. Fredlund DG, Rahardjo H, Rahardjo H. Soil mechanics for unsaturated soils. John Wiley & Sons  
583 1993.
- 584 [34]. Karamitros DK, Bouckovalas GD, Chaloulos YK. Insight into the seismic liquefaction  
585 performance of shallow foundations. J. Geotech. Geoenviron. Eng. 2013; 139(4):599–607.  
586 [https://doi.org/10.1061/\(ASCE\)GT.1943-5606.0000797](https://doi.org/10.1061/(ASCE)GT.1943-5606.0000797).
- 587 [35]. Sancio R, Bray JD, Durgunoglu T, Onalp A. Performance of buildings over liquefiable ground  
588 in Adapazari, Turkey. Proc., 13th World Conf. on Earthquake Engineering, Canadian Association  
589 for Earthquake Engineering, Ottawa 2004.
- 590 [36]. Zeybek, A., Madabhushi, S. P. G. Centrifuge testing to evaluate the liquefaction response of air-  
591 injected partially saturated soils beneath shallow foundations. Bulletin of Earthquake  
592 Engineering, 2017; 15(1):339-356.
- 593 [37]. Borchardt RD. Estimates of site-dependent response spectra for design (methodology and  
594 justification). Earthquake spectra 1994; 10(4):617-653. <https://doi.org/10.1193/1.1585791>.
- 595 [38]. Hardin BO, Drnevich VP. Shear modulus and damping in soils: design equations and curves.  
596 Journal of Soil Mechanics & Foundations Div 1972;98(7).
- 597 [39]. Arulanandan K, Scott RF. Verification of numerical procedures for the analysis of soil

598 liquefaction problems. In International Conference on the Verification of Numerical Procedures  
599 for the Analysis of Soil Liquefaction Problems 1993.

600 [40]. Zeghal M, Elgamal AW, Zeng X, Arulmoli K. Mechanism of liquefaction response in sand–silt  
601 dynamic centrifuge tests. *Soil Dynamics and Earthquake Engineering* 1999; 18(1):71-85.  
602 [https://doi.org/10.1016/S0267-7261\(98\)00029-3](https://doi.org/10.1016/S0267-7261(98)00029-3).

603 [41]. Adalier K, Elgamal AW. Seismic response of adjacent dense and loose saturated sand columns.  
604 *Soil Dynamics and Earthquake Engineering* 2002; 22(2):115-127.  
605 [https://doi.org/10.1016/S0267-7261\(01\)00059-8](https://doi.org/10.1016/S0267-7261(01)00059-8).

606 [42]. Brennan AJ, Thusyanthan NI, Madabhushi SP. Evaluation of shear modulus and damping in  
607 dynamic centrifuge tests. *Journal of Geotechnical and Geoenvironmental Engineering* 2005;  
608 131(12):1488-1497. [https://doi.org/10.1061/\(ASCE\)1090-0241\(2005\)131:12\(1488\)](https://doi.org/10.1061/(ASCE)1090-0241(2005)131:12(1488)).  
609

610 **Tables**

611

612 **Table 1** Index properties of Toyoura sand

Property	Value
Specific gravity, $G_s$	2.65
$D_{50}$ (mm)	0.19
$D_{10}$ (mm)	0.14
Maximum void ratio, $e_{max}$	0.973
Minimum void ratio, $e_{min}$	0.609
Void ratio @ $D_r = 50\%$	0.791
Permeability, $k$ (m/s)	$2 \times 10^{-4}$
Relative density, $D_r$	50 %
Sand	100 %

613

614 **Table 2** Properties of foundation-structure system

Property	Foundation and superstructure*	
	Buffer Tank	Flare Stack
Footing dimension	4 x 4 x 1 m <sup>3</sup>	4 x 4 x 2 m <sup>3</sup>
Material used	Aluminum	Aluminum
Mass of footing	44.8 ton	87.04 ton
Thickness of superstructure	6 cm	6 cm
Outer diameter of superstructure	1.6 m	1.6 m
Height of lumped mass	7.6 m	14 m
Lumped mass	28.16 ton	14.08 ton
Bearing pressure @ 40g	51.2 kPa	71.2 kPa
Design period of soil-structure system	0.4 s (2.5 Hz)	0.5 s (2 Hz)

\*All units are given in prototype scale

615

616 **Table 3** Distribution of different transducers within the model ground

Level	Transducers*	Location (prototype scale)		Initial effective stress ( $\sigma'_{vo}$ )		
		X	Z (depth)	Magnitude, kPa		Description
		m	m	Fully saturated**	Partially saturated***	
Level 1	P1, A1	12	10	91.60	93.56	Model centerline
Level 2	A2	12	8	63.12	65.08	Model centerline
Level 3	P2	18	6	50.42	52.38	Below FS footing
	P3, A3	12	6	51.64	53.60	Model centerline
	P4	6	6	46.72	48.68	Below BT footing
	P5	18	4	43.69	45.65	Below FS footing
Level 4	A4	12	4	31.16	33.12	Model centerline
	P6	6	4	36.69	38.65	Below BT footing
	P7	18	2	43.00	44.96	Below FS footing
Level 5	P8, A5	12	2	08.36	10.32	Model centerline
	P9	6	2	31.00	32.96	Below BT footing

617 \*A: acceleration transducers, P: pore pressure transducers

618 \*\*Water table in case of fully saturated model ground is 0.7 m (17.5 mm in model scale) below the top surface of model ground

619 \*\*\*Water table in case of partially saturated model ground is 0.9 m (22.5 mm in model scale) below the top surface of model ground

620

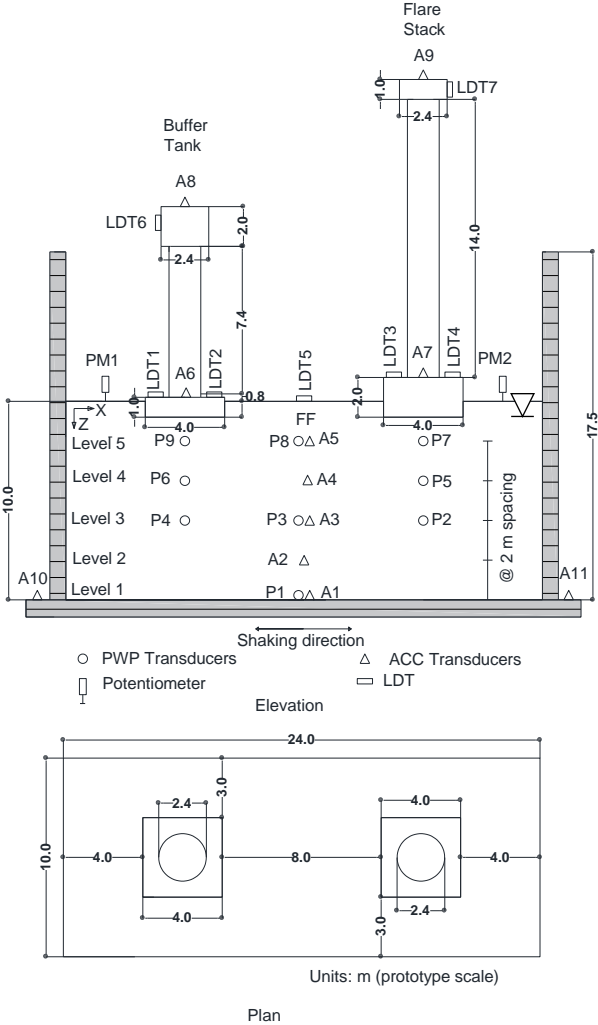
621 **Table 4** Test conditions and properties of applied main shakings

Model description	Test conditions		Peak acceleration of input ground motion ( $m/s^2$ ) in prototype scale	
	Relative density $D_r$ (%)	Degree of saturation $S_r$ (%)	Tokachi-Oki ground motion*	Tohoku ground motion**
Fully saturated model ground	53.1	99.1	1.51	7.1
Partially saturated model ground	51.8	88.4	1.7	7.3

622 \*Ground motion recorded at Hachinohe Port (NS component) during the 1968 Tokachi-Oki earthquake

623 \*\*Design earthquake motion for highway bridges in Japan (2-I-I-3, NS component) recorded at the ground surface near the New Bansuikyo Bridge,  
624 Tochigi during 2011 Tohoku earthquake

625



627

628     **Fig. 1. Centrifuge model layout**

629

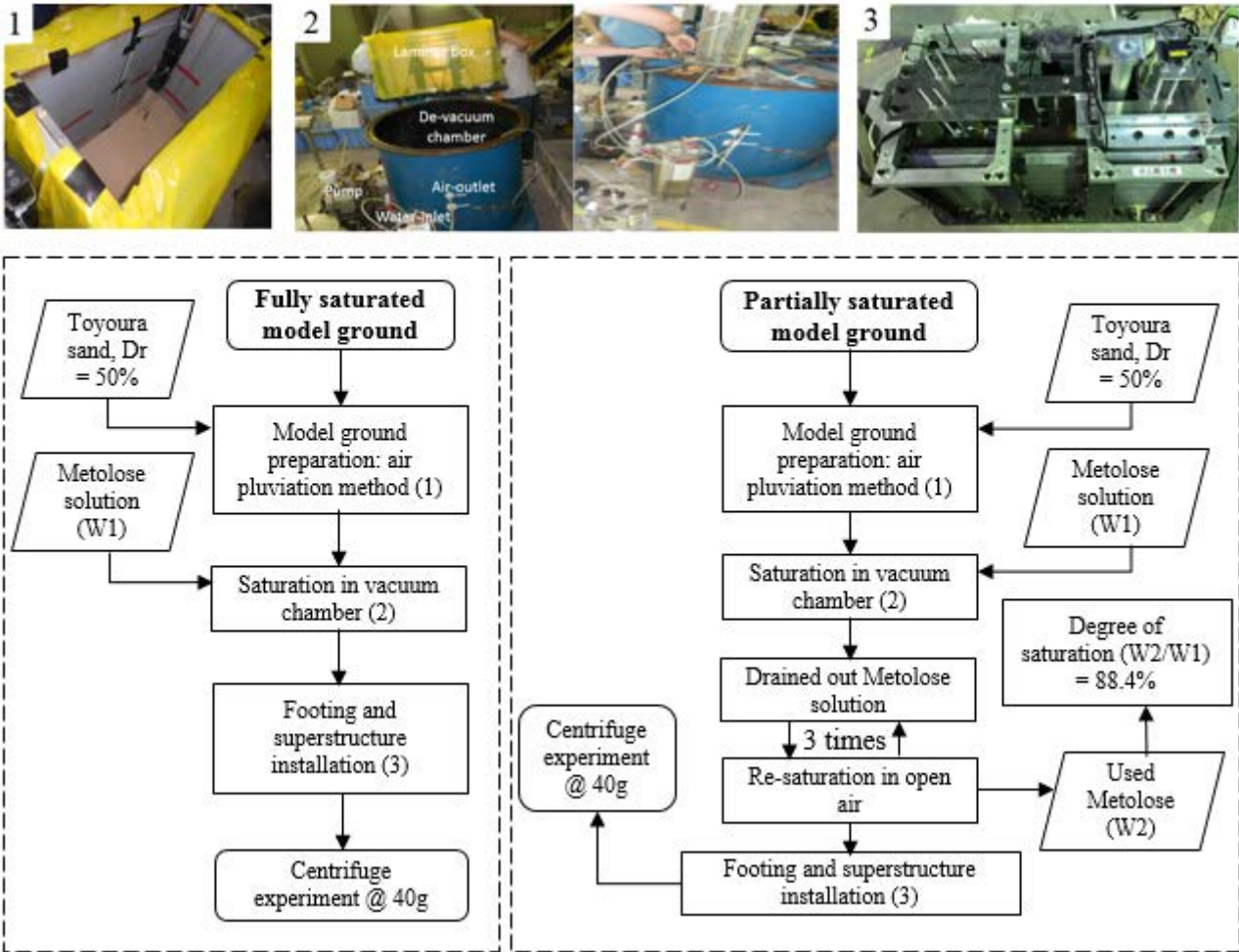


**Fig. 2.** Flow chart for fully saturated and partially saturated model ground preparation

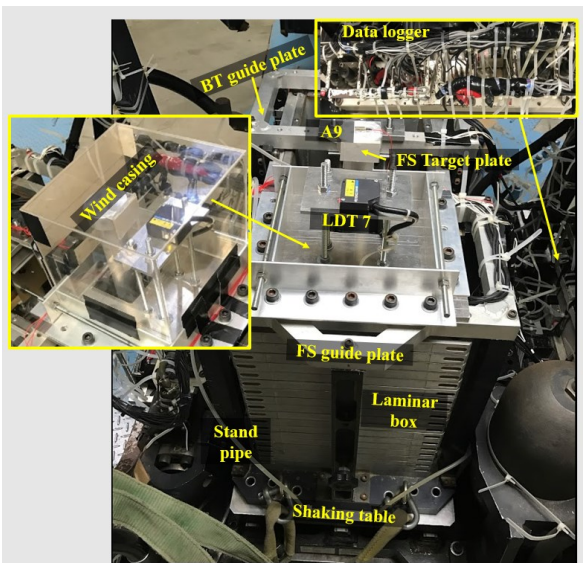


**Fig. 3.** Instrumented model setup mounted on centrifuge shaking table

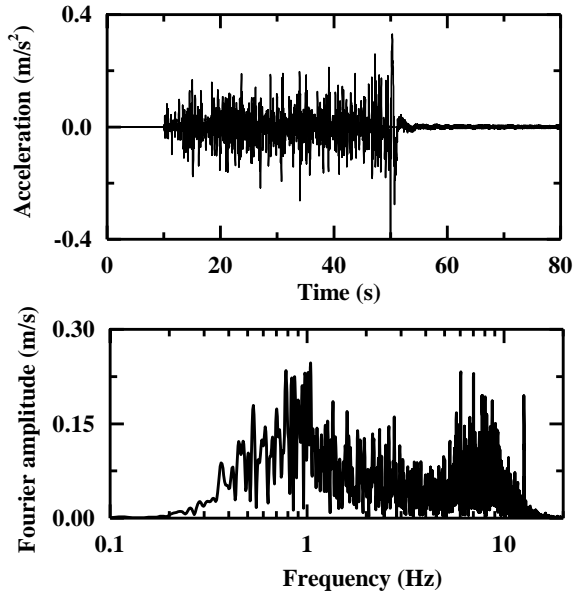


**Fig. 4.** Acceleration time history and Fourier spectra of input white noise (WN1) in prototype scale

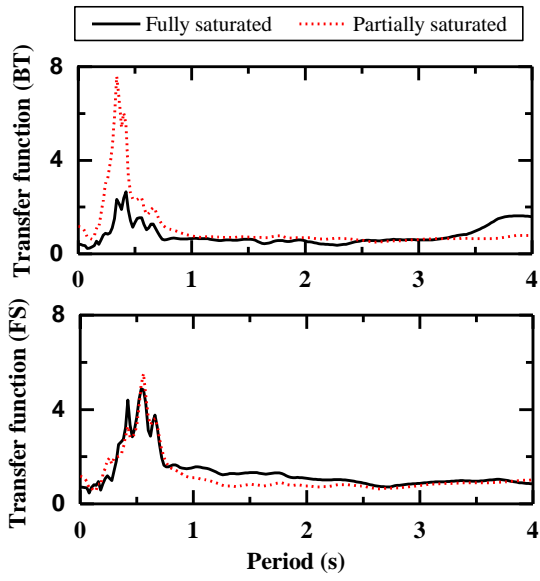


**Fig. 5.** Transfer Function obtained at top of Buffer Tank and Flare Stack in prototype scale



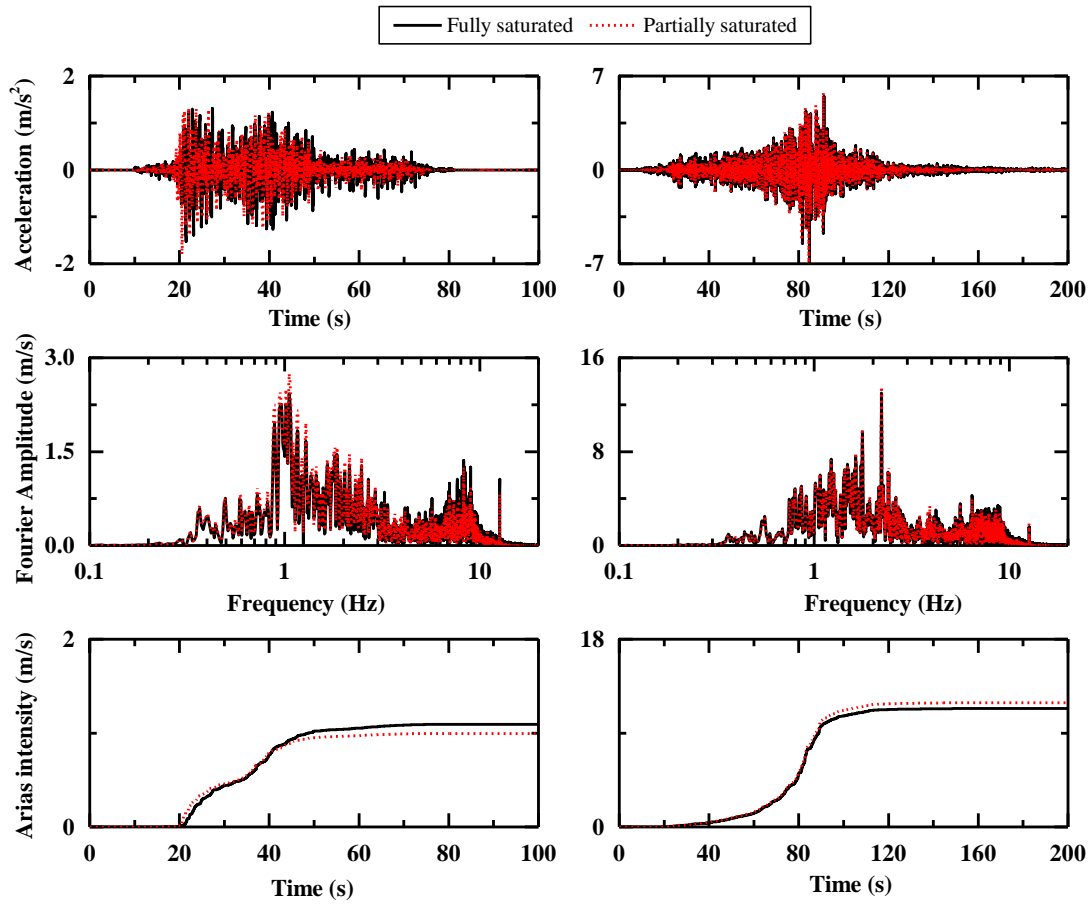


**Fig. 6.** Acceleration time histories, Fourier spectra and Arias intensities of Tokachi-Oki (left) and Tohoku (right) ground motions for both fully and partially saturated model grounds in prototype scale

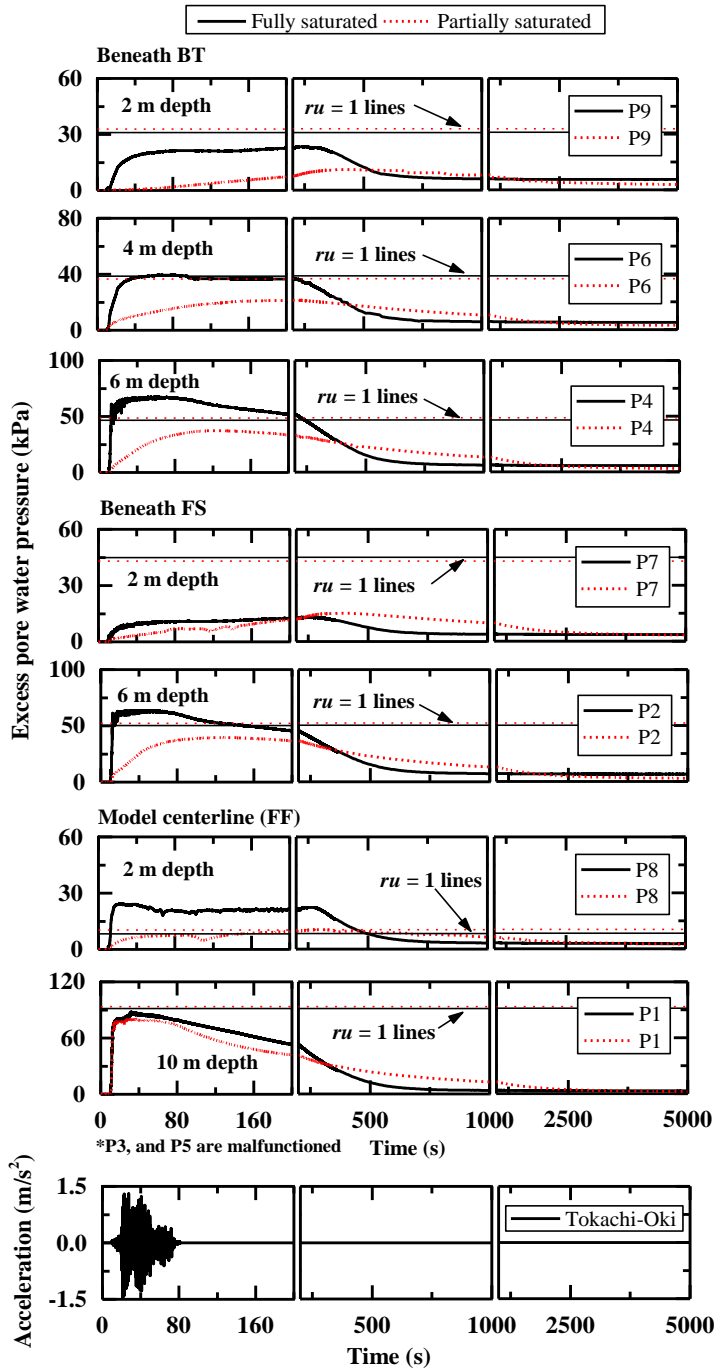


**Fig. 7.** EPWP time histories obtained during Tokachi-Oki ground motion

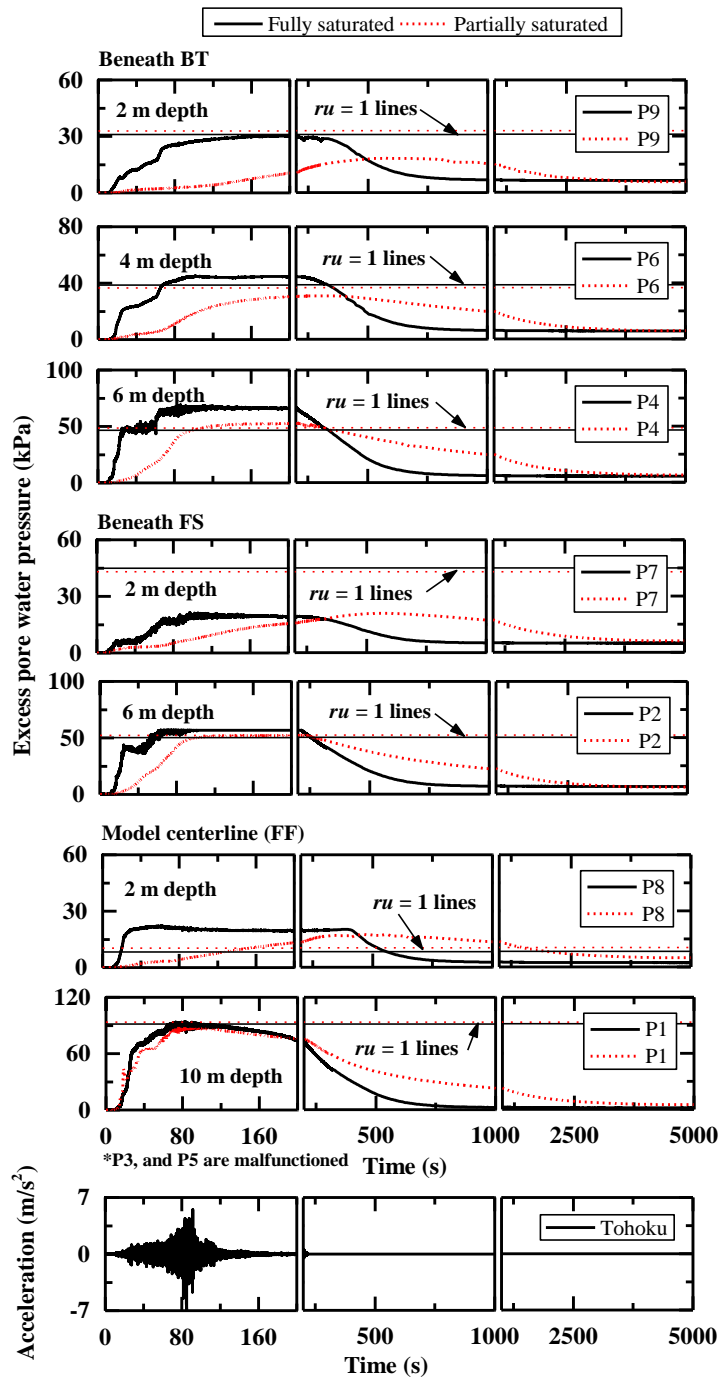


**Fig. 8.** EPWP time histories obtained during Tohoku ground motion

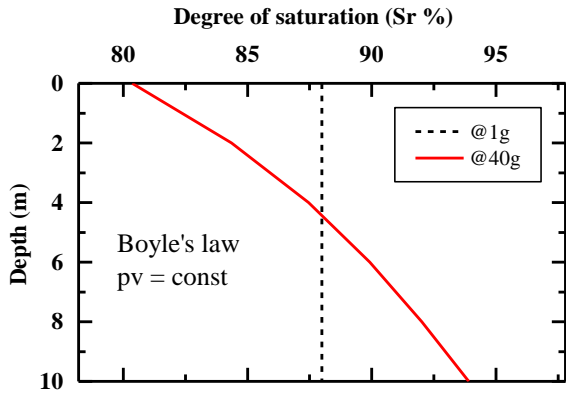


**Fig. 9.** Variation of degree of saturation within the partially saturated model ground

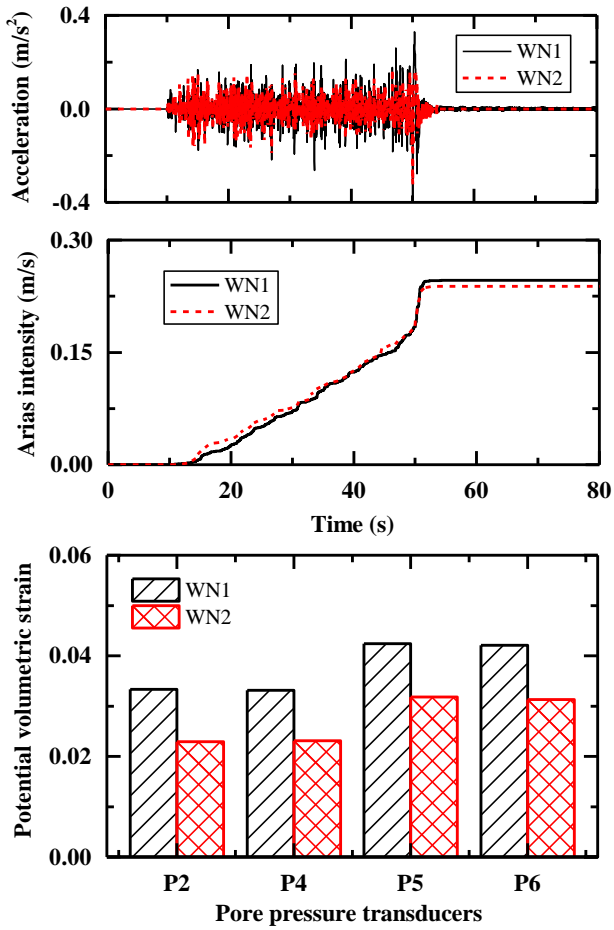


**Fig. 10.** Maximum potential volumetric strain during white noise 1 (WN1) and white noise 2 (WN2)

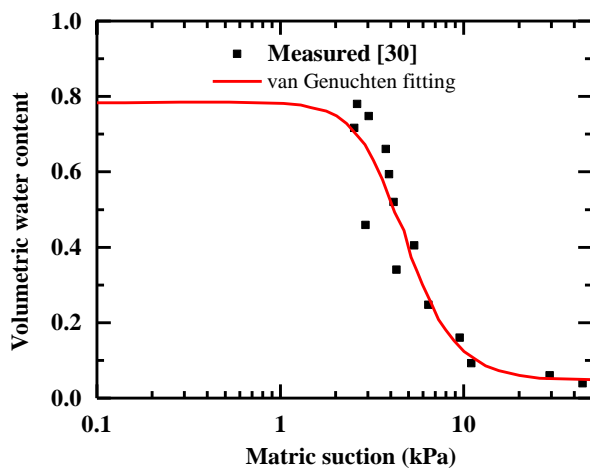
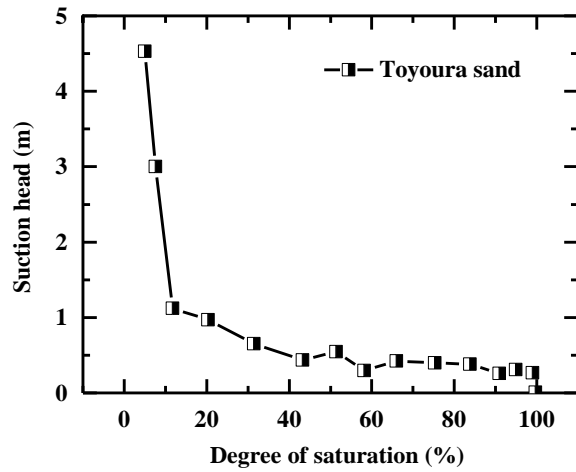


**Fig. 11.** Soil-water characteristic curve for Toyoura sand (after Unno et al. [30])

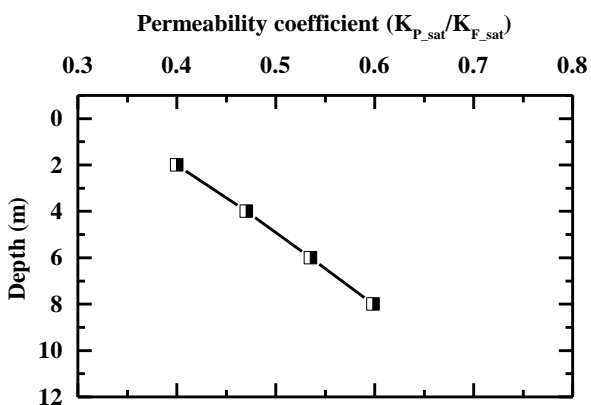


**Fig. 12.** Change in permeability because of induced partial saturation

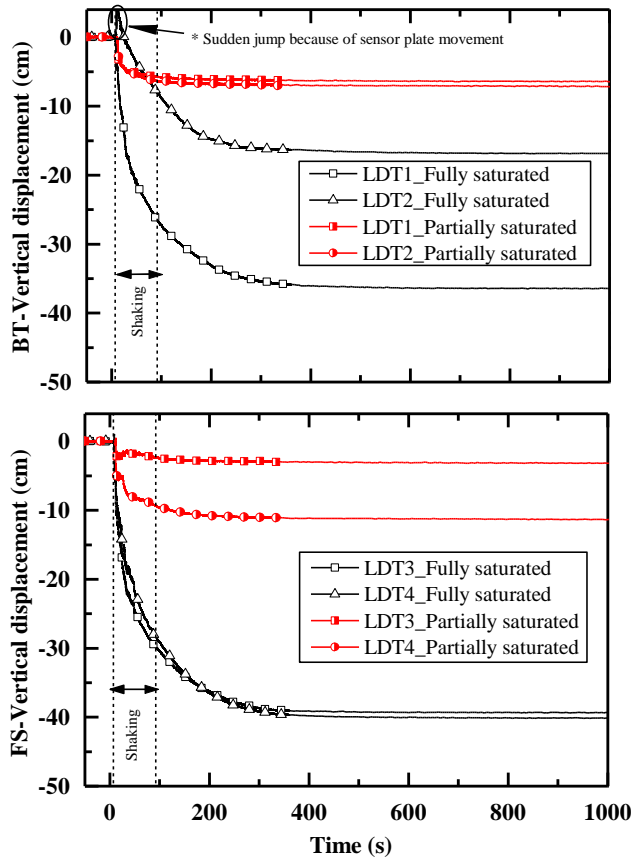


**Fig.13.** Settlement time histories of BT (LDTs 1 and 2) and FS (LDTs 3 and 4) during Tokachi-Oki ground motion

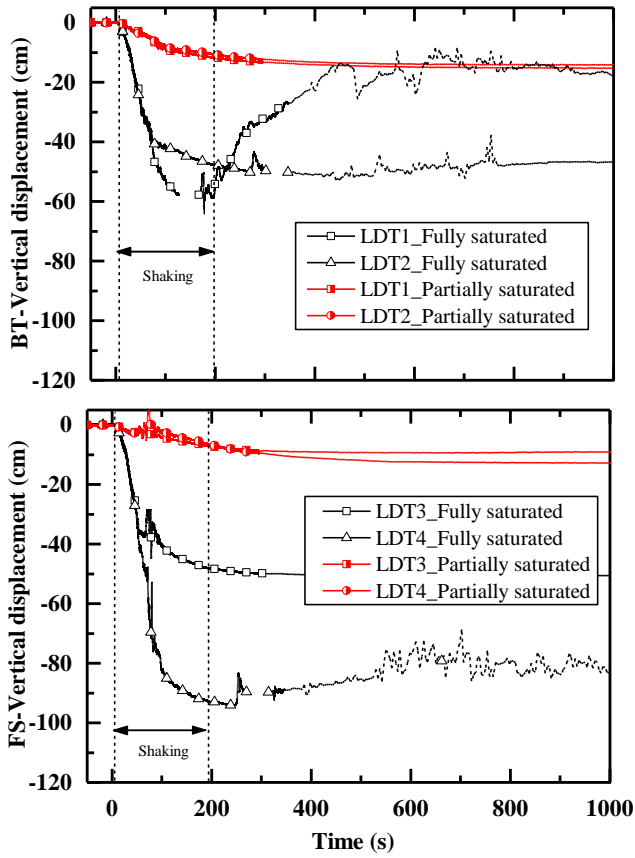


**Fig. 14.** Settlement time histories of BT (LDTs 1 and 2) and FS (LDTs 3 and 4) during Tohoku ground motion

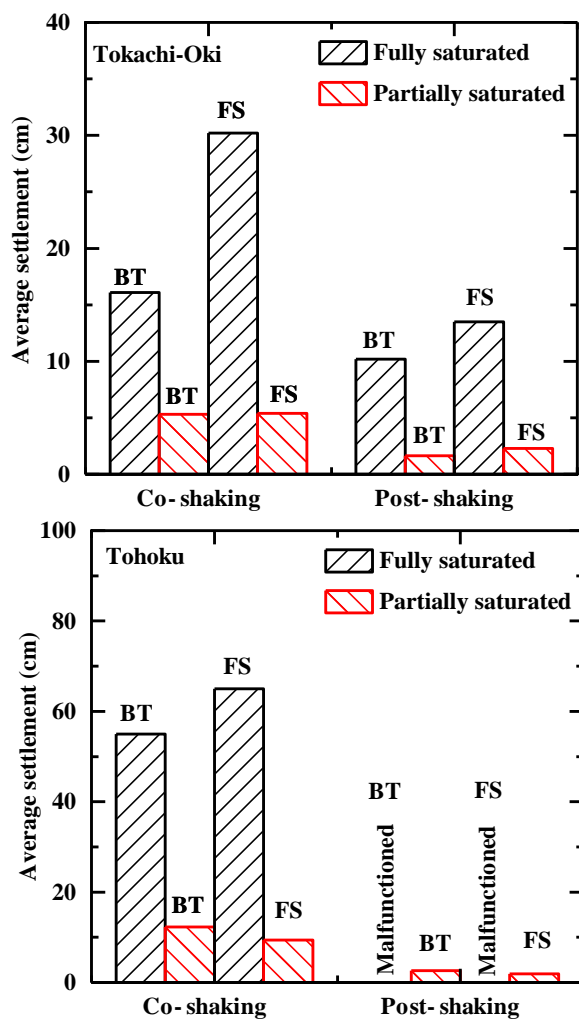


**Fig. 15.** Co-shaking and post-shaking settlement during Tokachi-Oki and Tohoku ground motion



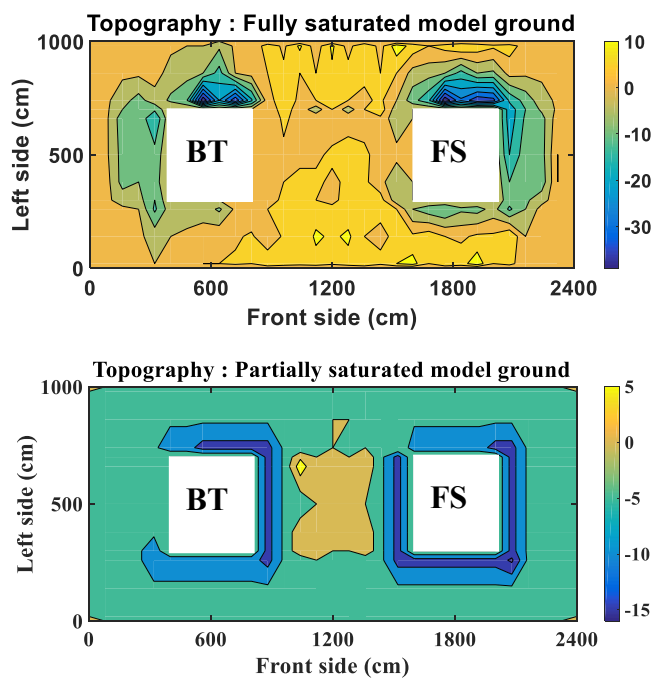


**Fig. 16.** Topography (surface settlement in cm) after the centrifuge experiment

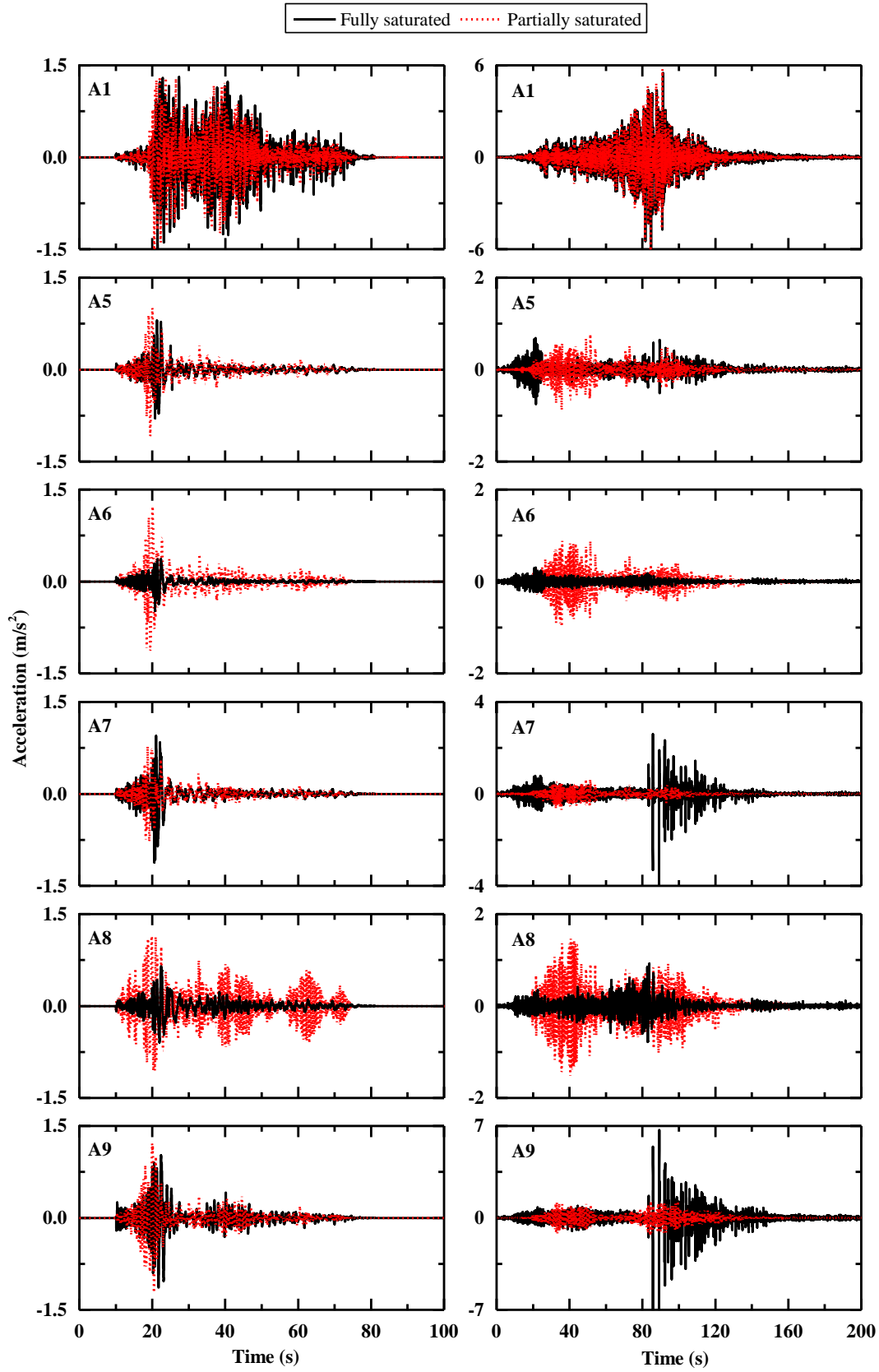


**Fig. 17.** Acceleration time histories during Tokachi-Oki (left) and Tohoku (right) ground motions

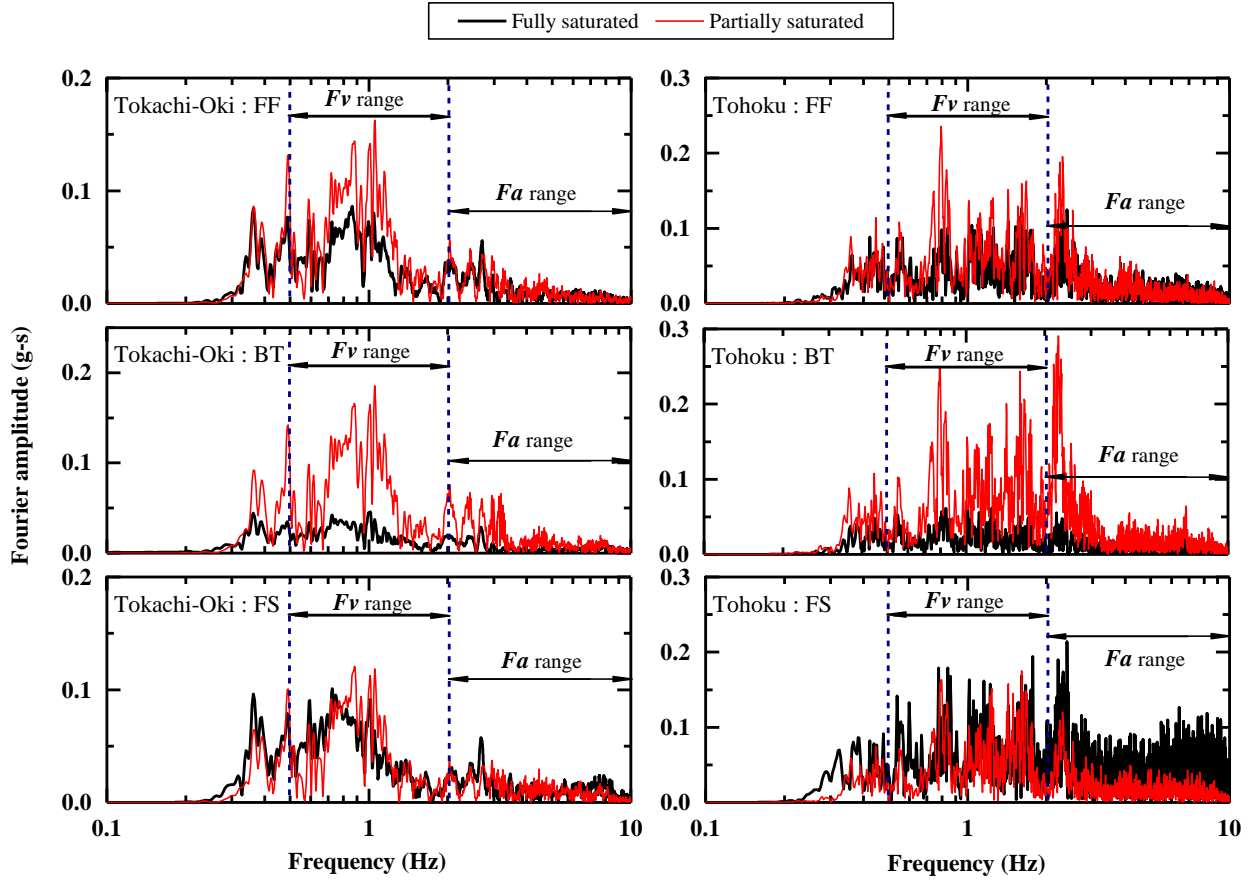


**Fig. 18.** Fourier amplitude spectra of acceleration recorded at footings of BT and FS and free field

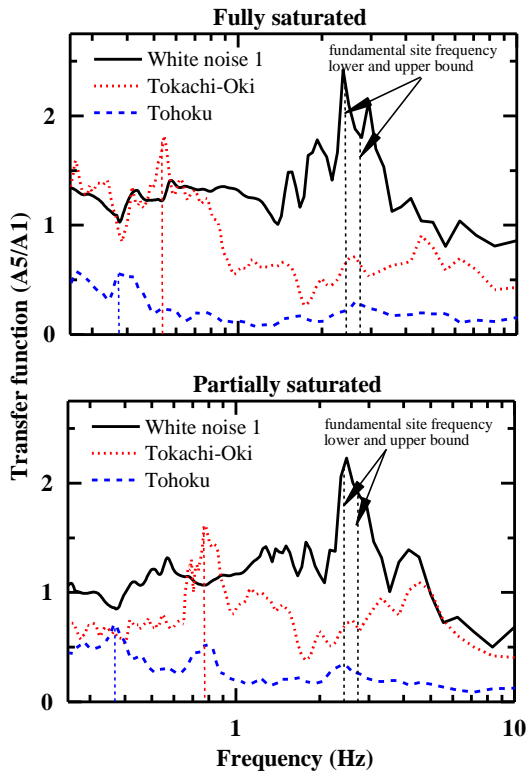


**Fig. 19.** Far-field model ground behavior during white noise, Tokachi-Oki, and Tohoku ground motions

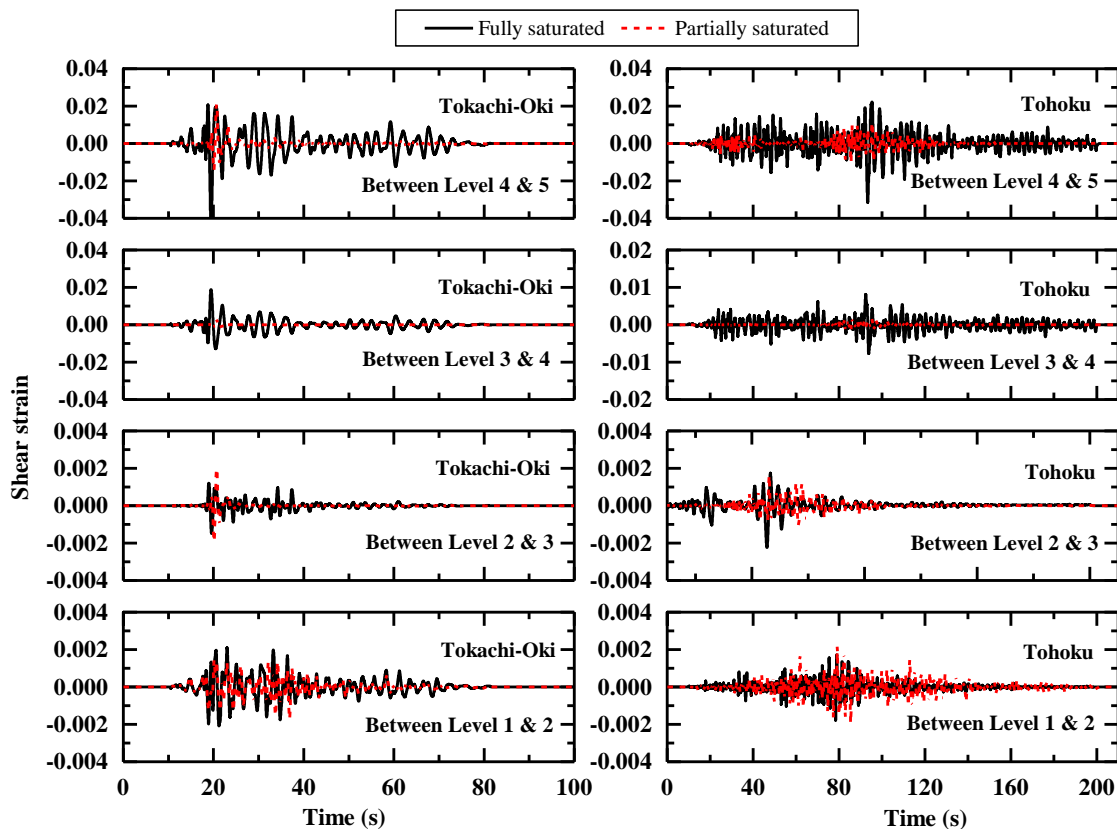


**Fig. 20.** Shear strain time histories along model centerline (MC) between different levels